3D printed silica-gelatin hybrid scaffolds of specific channel sizes promote collagen type II, Sox9 and Aggrecan production from chondrocytes

Maria Nelson[1], Siwei Li[1], Samuel J. Page[2], Xiaomeng Shi[1], Peter D. Lee[3], Molly M. Stevens[1,4,5], John V. Hanna[2], Julian R. Jones[1]

[1]Department of Materials, Imperial College London, London, SW7 2AZ, UK
[2]Department of Physics, University of Warwick, Gibbet Hill Road, Coventry CV4 7AL, UK
[3]School of Materials, University of Manchester, Manchester, M13 9PL, UK
[4]Institute of Biomedical Engineering Imperial College London, London, SW7 2AZ, UK
[5]Department of Bioengineering Imperial College London, London, SW7 2AZ, UK.

Abstract

Inorganic/organic hybrids have co-networks of inorganic and organic components, with the aim of obtaining synergy of the properties of those components. Here, a silica-gelatin sol-gel hybrid "ink" was directly 3D printed to produce 3D grid-like scaffolds, using a coupling agent, 3-glycidyloxypropyl)trimethoxysilane (GPTMS), to form covalent bonds between the silicate and gelatin co-networks. Scaffolds were printed with 1 mm strut separation, but the drying method affected the final architecture and properties. Freeze drying produced <40 μm struts and large ~700 μm channels. Critical point drying enabled strut consolidation and optimal mechanical properties, with ~160 μm struts and ~200 μm channels, which improved mechanical properties. This architecture was critical to cellular response: when chondrocytes were seeded on the scaffolds with 200 μm wide pore channels *in vitro*, collagen Type II matrix was preferentially produced (negligible amount of Type I or X were observed), indicative of hyaline-like cartilaginous matrix formation, but when pore channels were 700 μm wide, Type I collagen was prevalent. This was supported by Sox9 and Aggrecan expression. The scaffolds have potential for regeneration of articular cartilage regeneration, particularly in sports medicine cases.

Keywords: 3D printing; hybrid; articular cartilage; scaffold.

1. Introduction

Articular cartilage defects affect millions of people worldwide and treatment is currently limited to replacement with synthetic materials or regeneration through stimulation of fibrocartilage growth, e.g. via microfracture surgery [1]. Neither strategy restores the structure, properties nor function of hyaline articular cartilage as it has limited self-repair due to low cell density, low metabolism and absence of blood supply [2]. In young people, most joint problems begin with small lesions in the articular cartilage tissue due to wear and tear, trauma or sporting injures [3]. If the lesion is detected and surround by otherwise healthy cartilage, microfracture (or nanofracture) can be performed, in which small holes are made in

the subchondral bone to enable bone marrow to fill the defect, enabling some progenitor/stem cells to reach the defect site [4]. However, due to low numbers of progenitor cells in a heterogeneous population and lack of organisation, fibrocartilage results. With inferior mechanical and structural properties compared to hyaline cartilage, the repair tissue cannot sustain the loads of the articular joint and degeneration occurs, requiring repetition of the surgery [1].

Autologous matrix-induced chondrogenesis (AMIC) is a one-step approach that combines microfracture with a scaffold [5]. This type of approach has potential if the scaffold can promote Type II collagen matrix production and share load with the host cartilage. Currently, layered fibremat-like porcine collagen scaffolds, e.g. Chondro-Gide® (Geistlich Biomaterials, Switzerland), are used in the AMIC technique [6], but while some Type II collagen matrix was detected, clinical outcomes have been similar to microfracture without the scaffold [7]. Although clinical studies report positive patient [8], long term success of such material remains in doubt due the type of cartilage formed. Hydrogels have been used in modified AMIC animal studies [9], but they have low mechanical properties [10].

One strategy for improving the quality of articular cartilage regeneration is to develop a scaffold that has potential to modify the AMIC technique and regenerate full-thickness cartilage defects. In a modified procedure, a scaffold should provide a suitable environment for bone marrow stromal cells (MSCs) to become chondrogenic and produce hyaline cartilage extracellular matrix. The scaffold should have a stiffness conducive to cartilage formation and a similar response to mechanical loads as cartilage before degrading/remodelling as the native tissue structure develops [11-13]. The Chondro-Gide® scaffold has shown some success[9], but could be improved by tailored stiffness and pore architecture. The 3D pore architecture present within scaffolds used for cartilage tissue engineering also plays a vital role in tissue formation [13,14]. For example, efficient diffusion channels across a scaffold are essential to allow for full thickness infiltration of cells and extracellular matrix formation while avoiding waste build-up [15].

3D printing can provide accurate control over scaffold design. Printed scaffolds have been predominantly synthetic biodegradable polymers, such as poly(L-lactide), due to ease of 3D printing but they do not have suitable surface chemistry, stiffness or biodegradation rate [16]. New "inks" are required. The collagen used to produce Chondro-Gide® is difficult to print due to its low solubility[17]. Gelatin is a hydrolysed form of collagen and retains the information signals that may promote cell differentiation, e.g. the Arg-Gly-Asp (RGD) sequences [18]. However, scaffolds made of gelatin alone have poor mechanical properties, an order of magnitude lower than native cartilage, even when crosslinked in a dual network [19]. To stiffen

gelatin, silica-gelatin hybrid foam scaffolds were developed by Mahony *et al.* [20,21]. Sol-gel hybrids are co-networks of inorganic (e.g. silica) and organic (in this case gelatin), wherein the molecular level interactions enable them to retain strength from the inorganic and elasticity from the organic [22]. Mechanical properties and dissolution of the foam hybrids were tailored through covalent coupling between the inorganic and organic networks using 3-glycidyloxypropyl)trimethoxysilane (GPTMS), creating Class II hybrids [20,21]. Without such bonding, hybrids would dissociate rapidly on contact with water [23]. Silica/gelatin hybrids have also been produced as aerogels [24,25] and Blaker *et al.* produced fibrous silica/gelatin Class II scaffolds using a solution blow spinning technique, which gave precise control over fibre diameter [26]. Silica/gelatin scaffolds have been printed before [27], but covalent coupling, via 1-ethyl-(3-3-dimethylaminopropyl) carbodiimide hydrochloride (EDC) and N-hydroxy-succinimide (NHS), was not proven to be successful (little change in mechanical properties), with the hybrids either dissolving rapidly in simulated body fluids or the dissolution was not reported. Application to cartilage regeneration was also not investigated.

Recently, hybrids of silica, poly(tetrahydrofuran) (PTHF) and poly(ε-caprolactone) (PCL-diCOOH) [28], were 3D printed and *in vitro* cultures of ATDC5 murine chondrogenic cells in scaffolds with ~250 μm channel size produced collagen type II matrix, with negligible collagen type I or X produced. Scaffolds made solely of PCL with similar pore architectures did not provoke collagen Type II production. Similar results were seen with the more clinically relevant human stem cells, which differentiated down a chondrocytic route when cultured on the hybrid scaffolds with ~250 μm channel size, with Sox9, collagen Type II, and glucosaminoglycan (GAG) production [29], whereas large pores seemed to produce fibroblastic cells and collagen Type I matrix.

The aim here was to 3D print the first silica-gelatin hybrid with covalent coupling between the gelatin and silica network, and to investigate the effect of the degree of coupling and drying method (freeze drying versus critical point drying) on the architecture, structure and properties of the scaffolds. The potential of scaffold architectures for hyaline cartilaginous matrix production*in vitro*, particularly the effect of pore channel size, was assessed in culture with cartilage cells.

2. Materials and methods

2.1 Hybrid preparation

All reagents were supplied by Sigma Aldrich (Dorset, UK), unless otherwise specified. Hybrid preparation was modified (Figure 1a) from the procedure developed by Mahony *et al.* [20],

which used hydrofluoric acid (HF) catalysis to induce rapid condensation of the silica network to produce foam scaffolds. Here, a HF-free method with a slower condensation rate was required to allow 3D printing directly from sol. Initially gelatin (Bovine, Type A) was dissolved in 10 mM hydrochloric acid (HCl) at a concentration of 50 mg mL^{-1}. This solution was functionalised by addition of an appropriate amount of GPTMS to give molar ratios of GPTMS:gelatin (termed coupling factor, CF) ranging between 0–1000. The functionalised gelatin solution was left to mix (3 h or 14 h) before being added to the sol.

A sol was prepared by adding the following in order: deionised water, HCl (1 M) and tetraethyl orthosilicate (TEOS). The molar ratio of water: TEOS (R ratio) was 4 and HCl was added to catalyse TEOS hydrolysis at a volume ratio (water:HCl) of 3. The solution was stirred to allow hydrolysis of TEOS (1 h), before adding the functionalised gelatin. The gelatin:silica ratio, e.g. 70G:30SiO$_2$, (70G) describes the mass ratio of dry gelatin to SiO$_2$, under the assumption that 1 mole of TEOS forms 1 mole of SiO$_2$. Any silica contributions from GPTMS were ignored in this nominal ratio. Here, 60G, 70G, 78G and 84G compositions were investigated.

The functionalised gelatin and sol were monitored during mixing to assess printability of the hybrid inks. Some hybrids were prepared as monoliths by transferring the sol to moulds after 5 h mixing for further condensation of the silica network. The hybrid inks prepared for 3D printing were aged until the gels had adequate gel strength then 3D printed into scaffolds and aged. Hybrid monoliths and scaffolds were aged for 1 week and then dried by freeze drying or critical point drying.

The variables investigated to determine a new hybrid method and composition compatible with 3D printing were: CF (0-1000), functionalisation time (3 h or 14 h), sol aging temperature (21°C, 40°C), gelatin:silica ratio (60G-84G) and drying method (freeze drying or critical point drying).

Two drying methods were compared: freeze drying (FD), where samples were frozen at −18°C overnight then placed in a freeze dryer (Thermo Scientific Heto PowerDry LL1500) for 24 h at −96°C at a pressure of 0.13 mbar; critical point drying (CPD), where scaffolds were soaked at 3 h intervals in water-ethanol co-solvents with 10%-100% ethanol volume at 10% increments before the scaffolds were immersed in 100 % ethanol overnight. The CPD (Tousimis 931 Series, 2.5 in I.D Chamber) was used in 8 h Stasis Mode. The critical point is achieved at a critical temperature and pressure of 31°C and 1072 psi/173.9 bar for 2 minutes.

2.2 Verification of covalent coupling

The ninhydrin assay was used to determine the efficiency of the GPTMS coupling, and the degree of crosslinking in the hybrid, as it can quantify the number of primary and secondary amine units in a solution, which here would correspond to dissolved, uncoupled gelatin [30]. 2 mL of DI water was added to hybrid samples and gelatin standards in glass vials and held in a water bath for 1 h at 80°C, when 1 mL of ninhydrin reagent was added to each vial and left for 30 minutes. The samples and standards were cooled to room temperature and 5 mL of 95 % ethanol added. A further dilution of 1:49 sample/standard volume to additional ethanol volume was required. Absorbance values were measured using a microplate reader (SpectraMax M5) at 570 nm from a 48 well plate. From the calibration curve, the presence of free amino acids and hence unreacted gelatin was quantified. To calculate the crosslinking index (the degree of crosslinking in the hybrid), Eq. 1 was used, where respectively; C_i and C are the optical absorbance of the gelatin solution before and after cross-linking.

$$Crosslinking\ Index\ (\%) = \frac{C_i + C}{C_i} \times 100 \qquad \textbf{Eq. 1}$$

Solid state ^{29}Si MAS NMR measurements were performed at 7.0 T using a Bruker HD-300 spectrometer operating at a Larmor frequency of 69.62 MHz. These experiments were performed using a Bruker 7 mm HX probe which enabled a MAS frequency of 5 kHz to be implemented. Quantitatively reliable ^{29}Si MAS NMR data were acquired through the use of single pulse excitation experiments with ^{1}H decoupling during data acquisition. A ^{29}Si $\pi/2$ pulse time of 5.5 µs was calibrated on solid kaolinite and all experiments employed $\pi/4$ pulse time of 2.75 µs, long recycle delays of 240 s, and a ^{1}H decoupling field of ~80 kHz during FID acquisition. Each ^{29}Si chemical shift was referenced to TMS (δ 0.0 ppm) via the secondary solid kaolinite reference (δ −92 ppm). The simulation, deconvolution and measurement of the relative resonance intensities from each spectrum was undertaken using the OriginPro software package and the network condensation was calculated according to Equation 2 [31]:

$$D_c = \frac{T^1 + 2T^2 + 3T^3}{3} + \frac{2Q^2 + 3Q^3 + 4Q^4}{4} \qquad \textbf{Eq. 2:}$$

where Q^n is the abundance of Q^n species and T^n is the abundance of T^n species. A T^n species consists of a Si atom with one Si-C bond and n bridging oxygen (-Si-O-Si-) bonds and 3-n non-bridging oxygen bonds. A Q^n species consists of a Si atom with n bridging oxygen bonds and 4-n non-bridging oxygen bonds.

Thermal gravimetric analysis (TGA) was carried out on a Netzsch (Selb, Germany) STA 449C between 21°C and 800°C, ramp rate of 10 K min^{-1}, air flow rate 50 mL min^{-1}, in an alumina crucible (n=3).

2.3 Developing hybrid 3D printing inks

The printing process was developed by adapting an Ultimaker Original (Ultimaker, The Netherlands) (Figure 1b). The filament reel was removed and a 10 mL Luer lock BD Plastipak™ syringes with tapered printing tips attached to the printing head. Gels were held in the syringe and the deposition rate (0.1 mL min^{-1}) was controlled by a PHD Ultra syringe pump (Harvard Apparatus, Holliston, MA). A 40 °C heater was placed around the syringe to ensure the gelatin component did not transition from liquid to solid prior to printing. From the syringe, the hybrid flowed along tubing (Harvard Apparatus PolyE polyethylene tubing with ID of 1.78 mm) towards the printing tip. A stainless steel dispensing tip (Nordson EFD, OD 1.83 mm) connected the syringe to the tubing and Ibidi male Luer connectors connected the tubing to the tapered printing tip (Nordson EFD ID 0.2 mm), which was attached to the 3D printer. The printing parameters were: 1 mm strut separation, 0.3 mm layer height, print head speed of 500 feed rate.
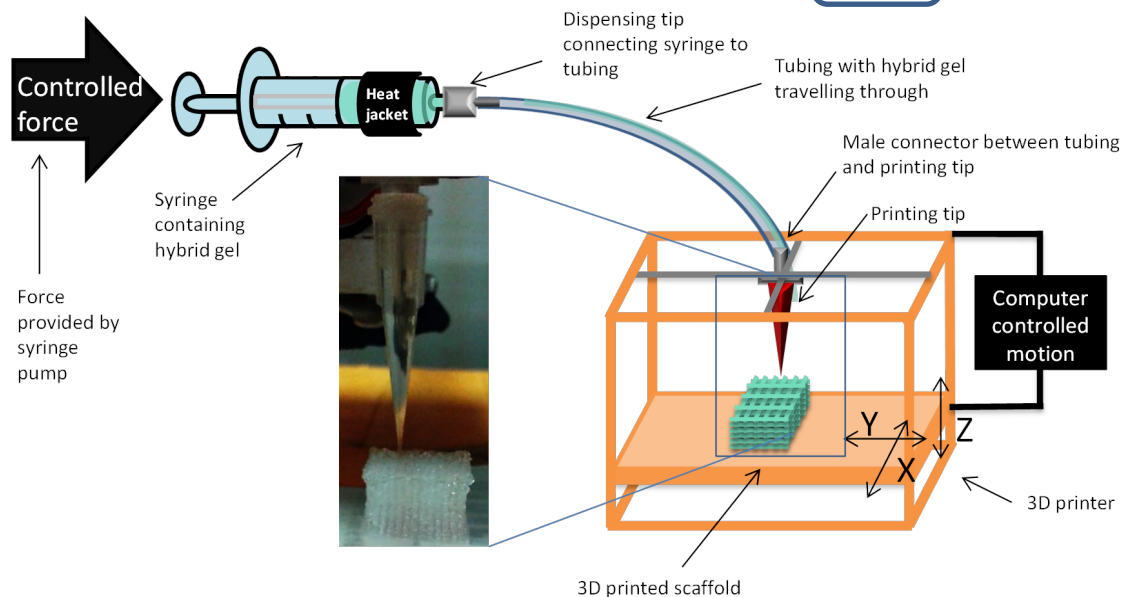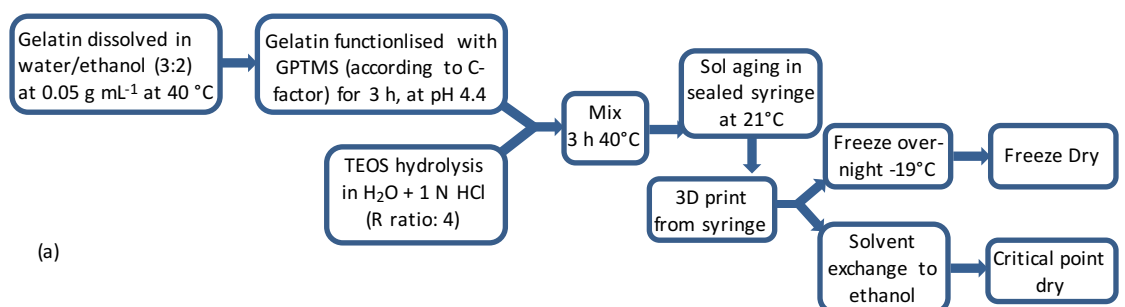
Figure 1. Schematics of (a) the sol-gel hybrid synthesis method; (b) the 3D printing set-up including an image of scaffold being 3D printed (inset).

On exiting the nozzle, the gels were required to hold their shape and scaffolds were built layer-by-layer without collapse. This required the gel to be in a specific gel strength range, termed "printing window". The hybrid inks were classified into 3 stages: i) not gelled enough for printing, "sol-aging"; ii) printable, the "printing window"; iii) too gelled for printing, "over-gelled". The timeframe for each stage of hybrid gelation was investigated, the solutions were monitored and 3D printing was attempted regularly (1 h intervals).

Rheometry of the ink was critical for printing. The storage and loss modulus of 78G CF 500 hybrid inks were measured at: 7, 9, 11, 13, 15 h after mixing. A Discovery Hybrid Rheometer, TA instruments (New Castle, US), was used in oscillatory mode. First, the Linear Viscoelastic Region (LVR) of the material was determined by an oscillation-amplitude test (0.1-100 % strain rate) performed under the conditions: 1 mm gap, 40 mm stainless steel plate, 40°C, 30 s soak time, 10 rad s^{-1} frequency using a solvent trap. A 10 % strain was found to be within the LVR so oscillation-frequency tests (0.1-100 Hz) were performed under the conditions: 1 mm gap, 40 mm stainless steel plate, 40°C, 30 s soak time, 10 % strain.

2.4 Characterisation of 3D printed scaffold

Skeletal (strut) density (ρ_s) values were obtained by helium pycnometry (Quantachrome Ultrapycnometer, measured 20 times in triplicate). Percentage porosity (φ) was calculated according to Eq. , where ρ_t is the total/bulk scaffold density (measured geometrically) and ρ_s is the skeletal density:

$$\text{Porosity}, \varphi \; = \left(1 - \frac{\rho_t}{\rho_s}\right) \times 100 \qquad \qquad \textbf{Eq. 3:}$$

Samples were coated in 5 nm chromium (Quorum, Q150T) and secondary electron images were obtained using a JEOL JSM 6010 SEM in normal scanning mode with an accelerating voltage of 20 kV, working distance of 19 cm, spot size of 50. Channel width and strut width were measured using ImageJ software (30 struts and 30 channels per sample, three samples).

X-ray microtomography (μCT) 3D reconstructions of the scaffolds were generated from tomographs at the Diamond Manchester Imaging Beamline I13 under the conditions of 0.1° intervals, 1 s exposure, 12 keV beam energy. The tomographs obtained were then layered

and rendered using Avizo software to generate the 3D reconstructions of the scaffolds and the internal pores.

Dissolution in Tris(hydroxymethyl) aminomethane (Tris) buffer solution was investigated. Tris buffer was prepared by dissolving 6.118 g of Tris in 1000 mL of distilled water. The pH was adjusted to 7.4 by addition of 1.0 M HCl at 36.5°C. 150 mg of dried scaffold was immersed in 100 mL of Tris solution (n = 3), as recommended [32]. At each of the 12 time points, 1 mL solution was removed for inductively coupled plasma optical emission spectroscopy analysis (ICP, Thermo Scientific iCAP 6300, flow rate of 1.5 mL min^{-1} and plasma power of 1300 W with auto sampler (ASX-520) (n = 3)) and 25 µL aliquots for gelatin detection by BCA assay (standard procedure using Pierce Micro BCA protein assay (n = 3), with gelatin solution standard and 4 h incubation). The removed solution was replenished with fresh Tris solution.

Compression testing was carried out using a TA ElectroForce® 3200 Series III, on 1:1 cube scaffolds (n = 8), using a 440 N load cell and compression rate of 0.5 mm min^{-1}.

2.5 Cell culture

All cell culture reagents were obtained from Invitrogen and Sigma-Aldrich (UK) unless specified otherwise. ATDC5 cell line (ATCC, UK) was culture expanded in basal DMEM supplemented with 5 % (v/v) FCS (foetal calf serum), 1 % (v/v) penicillin/streptomycin and 1 × ITS liquid supplement. Pre-osteoblast cell line MCT3T3 cells were culture expanded in basal α-MEM supplemented with 10 % (v/v) FCS and 1 % (v/v) penicillin/streptomycin. Upon confluence, cells were passaged using 500 µg mL^{-1} trypsin-EDTA (ethylene diamine tetra-acetic acid).

2.5.1 Cell viability

The *in vitro* cytotoxicity of the material was examined by assessing the metabolic activity of ATDC5 and MCT3T3 cells after exposure to the dissolution products of the 78G CF 500 material, in accordance to ISO 10993-5 and ISO 10993-12. Dissolution products released by the powder form of the 78G CF 500 (0.2 g mL^{-1} in DMEM and α-MEM at 37°C) over a 72 h period were prepared. Medical grade polyethylene (PE) was used as non-cytotoxic negative control and polyurethane (PU) containing 0.1 % (w/w) zinc diethyldithiocarbamate (ZDEC) was used as positive control, which induces reproducible cytotoxic response. The dissolution products were filter sterilised and dilution series (25 %, 50 %, 75 % and 100 %) were prepared and mixed with basal supplements prior to use in cell viability assays.

Cell viability was assessed by a calorimetric based on the conversion of 3-(4,5-dimethylthiazol-2-yl)-2,5-diphenyltetrazolium bromide (MTT) into formazan. The cells were

seeded at 1×10^4 cells per well on 96-well plates and left to grow in respective basal media for 24 h. The media was replaced with fresh basal media, dissolution products of 78G CF 500 scaffolds or controls and cultured for a further 24 h. The culture media was removed and MTT diluted in serum-free media (1 mg mL^{-1}) was added. Following an incubation period of 2 h, the MTT solution was replaced with 100 μL DMSO and shaken briefly to dissolve the formazan derivatives. The optical density was measured spectrophotometrically at 570 nm using a microplate reader (SpectraMax M5).

2.5.2 Cell attachment

A cell attachment study was performed using ATDC5 and MCT3T3 cell lines on the 78G CF 500 3D printed scaffolds (approximately $5 \times 5 \times 2$ mm^3). The scaffolds were sterilised with 70 % ethanol, washed with copious amount of PBS and placed into sterile 50 mL centrifuge tubes fitted with filter caps. 5 mL of cell suspension containing 3×10^6 cells in basal media was added to each centrifuge tube containing the scaffolds and incubated for 2 h, with gentle agitation every 30 minutes to allow for diffusion and well-distributed cell adhesion. Cell-seeded scaffolds were collected on day 3 and analysed for cell attachment by immunohistochemistry staining for cytoskeletal protein.

2.5.3 Cartilaginous matrix formation

A 28 day cartilaginous matrix formation study using ATDC5 cells was performed on scaffolds with two channel widths: 200 μm (CPD) and 700 μm (FD). The number of cells were adjusted as per the difference in volume of the scaffolds: 3×10^6 cells (for 200 μm channel width) or 10×10^6 (for 700 μm channel width) cells were seeded as described above. On day 3, basal DMEM was replaced by chondrogenic media and cultured for further 28 days with media change every 3-4 days. The chondrogenic media was made up of DMEM supplemented with 10 ng mL^{-1} rhTGF-β3 (100-36E, PeproTech, UK), 100 μM (28.95 μg mL^{-1}) L- Ascorbic acid 2-phosphate, 10 nM (3.92 ng mL^{-1}) dexamethasone and 1× ITS liquid supplement, a modification of the media described in previous studies [33,34]. After 28 days, the seeded scaffolds were analysed for chondrogenic differentiation and cartilaginous matrix formation.

2.5.4 Immunohistochemistry

Cell-seeded constructs were fixed with 4% paraformaldehyde (PFA) at day 3 or 28 and used for immunohistochemical analysis of cell attachment and cartilaginous matrix formation. Following permeabilisation with buffered 0.5% (v/v) Triton X-100 in PBS (300 mM sucrose, 50 mM NaCl, 3 mM MgCl$_2$, 20 mM HEPES and pH 7.2) and blocking with 10 mg mL^{-1} BSA in PBS, samples were incubated with relevant primary antiserum at 4 °C overnight. This was

followed by hour-long incubation with Alexa Fluor® 488-conjugated secondary antibody. Cytoskeletal marker anti-Vimentin antibody (rabbit polyclonal, IgG, Abcam, Cambridge, UK) was used at a dilution of 1:500 dilution in 10 mg mL^{-1} BSA in PBS. Chondrogenic differentiation and cartilaginous matrix markers, anti- Sox9, Aggrecan, Collagen Type II, Collagen Type I and Collagen Type X antibodies were used at dilutions of 1:150, 1:500, 1:500, 1:1000 and 1:100 respectively. F-actin was labelled using CytoPainter F-actin staining kit (Abcam, Cambridge, UK) following the manufacture's instruction. Briefly, Alexa Fluor® 568-conjugated phalloidin (1:1000 dilution in labelling buffer) was added simultaneously with the secondary antibody during the incubation period. All samples were counter-stained with DAPI (0.1 µg mL^{-1} in PBS) and imaged under confocal microscopy (Leica SP5 MP laser scanning confocal microscope and software, Leica Microsystems, Wetzlar, Germany).

2.5.5 Gene expression analysis

Day 28 constructs were lysed and total RNA was extracted using Qiagen RNeasy kit (Qiagen, UK) following maunfacturer's instructions. The RNA samples were treated with DNase-1 reagent and reverse-transcribed using the SuperScript® VILO™ kit (Invitrogen, UK). qPCR assays were carried out using the QuantStudio™ 6 Flex system (Thermo Fisher, UK) for analysing the expression genes including: *Sox9* (F: 5'-ctgaagggctacgactggac-3'; R: 5'-gaggaggaatgtggggagtc-3'), *Aggrecan* (F: 5'-aggaggtggtactgctggtg-3'; R: 5'-tctcactccagggaactcgt-3'), *Col2a1* (F: 5'-agtcaagggagatcgtggtg-3'; R: 5'-cgtcgtgctgtctcaaggta-3'), *Col1a1* (F: 5'-gagaagtctcaagatggtggc-3'; R: 5'-gcggggtcggagccctcgctt-3'), *Col10a1* (F: 5'-gccaagcagtcatgcctgat-3'; R: 5'-gacacgggcatacctgttacc-3'). The expression of genes of interest was normalised to the endogenous control GAPDH (F: 5'-gggtggagccaaacgggtc-3'; R: 5'-ggagttgctgttgaagtcgca-3'). The relative transcript levels of genes of interest were analysed using the comparative C_T method ($\Delta\Delta C_T$ method). Statistical analysis was performed at the level of ΔC_T.

2.5.6 GAG quantification

The quantity of sulphated GAGs synthesized by cells following 28-day culture on 78G CF 500 scaffolds was determined using the DMMB assay [35]. Day-28 samples were digested overnight at 60 °C with papain (working solution of 0.7 U papain prepared in papain buffer containing 8.2 mg mL^{-1} sodium acetate, 37 mg mL^{-1} disodium EDTA and 0.79 mg mL^{-1} cysteine hydrochloride in potassium phosphate buffer consisting of 27.2 mg mL^{-1} monobasic potassium phosphate and 34.8 mg mL^{-1} dibasic potassium phosphate, pH 6.4). 20 µL of the diluted extract (1:10 dilution in papain buffer) was then mixed with 200 µL DMMB reagent (16 µg mL^{-1} DMMB, 2 mg mL^{-1} sodium formate, 0.5 % (v/v) ethanol and 0.2 % (v/v) formic acid) and optical density of the resultant solution was measured at 540 nm. The GAG

content for each sample was normalised to the weight of blank scaffold measured on day 0. Results were expressed as mean ± SD.

3. Results

3.1 Hybrid ink composition and structural evolution

Efficacy of the covalent coupling by GPTMS between the silica and gelatin networks was investigated using the ninhydrin reaction to test for free amino acids and by applying Equation 1. Importantly, covalent coupling was successful using GPTMS. The degree of crosslinking increased linearly as C-factor increased from CF 0 to CF 500 (Figure 2a), however the increase in crosslinking, relative to amount of GPTMS added, was reduced as C-factor increased above CF 500. To avoid excess GPTMS in the hybrid system, a CF 500 was used for the silica-gelatin hybrid inks to determine the printing window.

Definition of the "printing window" is that within the printing window, the hybrid ink has sufficient viscosity that enabled the ink to retain its shape after extrusion from the syringe and onto the substrate, but the viscosity is not so high that the ink cannot be extruded from the syringe. The ink was able to be laid down layer-by-layer and resulting scaffolds were stable 3D printed structures. As gelatin content in the ink increased, the sol aging time and printing window widened (Figure 2b). A composition of 78G CF 500 was most efficient for use with the printing method as it required 8 h of sol aging (additional time it was left in a sealed container after the 3 h mixing of the silica sol and functionalised gelatin prior to printing), after which the ink was able to be 3D printed for 4 h. The storage and loss modulus measured between 7 h and 15 h of sol aging indicated an increasingly crosslinked gel which displayed no shear thinning behaviour (Figure S1). Direct writing or Robocasting techniques usually rely on the ink having shear thinning behaviour [36]. Instead, the ability to print came from the gel strength rather than viscoelastic behaviour. Rather than flowing through the tubing and nozzle, the highly crosslinked hybrid gel was forced under controlled pressure along the tubing and was able to hold its shape on exiting the nozzle.
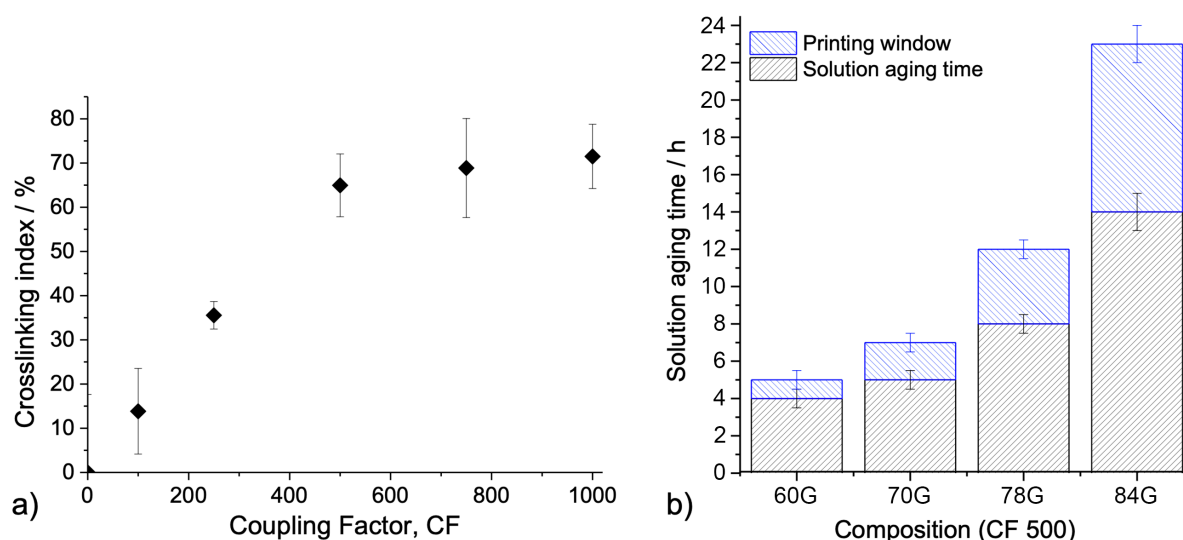
Figure 2. Determining the most suitable silica-gelatin hybrid composition for 3D printing inks: a) crosslinking index as a function of CF (molar ratio of GPTMS to gelatin); b) solution aging time and printing window of hybrid inks (CF 500) with respect to gelatin content.

A functionalisation time for gelatin with GPTMS of 3 h was selected as it reduced the rate of gelation, when mixed with the silica sol, maximising the time that the ink was within the printing window. The aging temperature was reduced from 40°C to 21°C to prevent collapse of the scaffolds due to flow of gelatin. The adapted method for printing was therefore: 3 h functionalization (CF 500) and 1 week aging at 21°C.

The effect of a reduced functionalisation time and aging temperature on the evolution of the hybrid structure for 78G CF 500 hybrids were assessed by solid state ^{29}Si MAS NMR (Figure 3). The 78G CF500 hybrids were produced using four different methods, one of which was the previously developed sol-gel foaming that used hydrofluoric acid (HF) to accelerate gelation of the silicate [20]. Method A was the newly developed method for the 3D printing ink: 3 h functionalisation with room temperature aging; Method B used a 14 h functionalisation, as did Methods C and D; in Method C gelation was accelerated with the addition of HF; and Method D was the sol-gel foaming method, gelled with HF, with an elevated aging temperature of 40ºC. Table 1 shows quantification of the relative proportions of the T^n species, Q^n species and degree of connectivity (D_c).
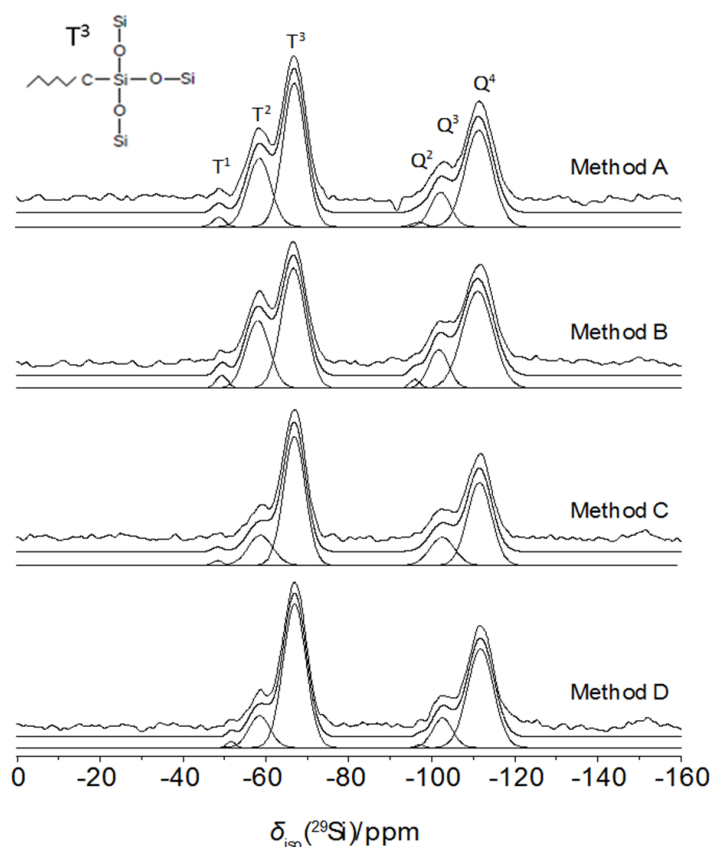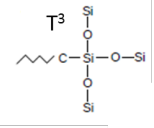
Figure 3. ^{29}Si solid state single pulse MAS NMR spectra for Methods A, B, C, and D with a schematic of the T^3 structure (inset). Method A = 3 h GPTMS functionalisation, printed; Method B = 14 h GPTMS functionalisation, printed; Method C : 14 h GPTMS + HF, printed; 14 h GPTMS functionalisation + direct foaming (no printing) + HF, aged at 40°C.

The longer functionalisation time resulted in a similar D_c (~90 %) as T^3 decreased from 39 % to 34 % and Q^4 increased from 32 % (Method A) to 35 % (Method B). Adding HF catalysis (Method C) caused a ~4 % increase in D_c, the most significant increase in D_c of all the parameters investigated. HF affected the T structure, as the relative proportion of T^1 more than halved for Method C; T^2 decreased from 19 % to 12 %; and T^3 increased from 34 % to 45 %. As aging temperature increased (Method D), Q^4 increased from 32 % to 36 %, as the higher temperature allowed gelatin chain movement and further condensation of the silicate, but D_c was similar. Aging at 40°C also caused 3D printed scaffolds to collapse, due to flow of the gelatin. As use of HF would complicate the process, and longer functionalisation time was not beneficial, Method A was taken forward for printing.

The results agreed with FTIR spectra (Figure S2), which showed 3 h functionalisation time to reduce Si-O-Si bonding prior to TEOS addition into the hybrid system, as band ratios for Si-O-Si compared to the Si-C band were 2.2 and 2.5 when for 3 h and 14 h respectively.

Table 1. T structure, Q structure, and degree of condensation quantified by ^{29}Si MAS NMR for hybrids synthesised using four different methods: A, B, C, and D. The composition of all hybrid are 78G CF 500. Insert shows the chemical structure of a silicon T^3 species (silicon in GPTMS with 3 bridging oxygens).

			Method A	Method B	Method C	Method D
			Ink method, 3 h functionalization	A + 18 h functionalisation time	B + HF addition	Foaming method using HF, plus aging at 40°C
Parameters	Functionalisation time /h		3	14	14	14
	Solution-aging /h		Until gelled	Until gelled	1	1
	HF addition		No	No	Yes	Yes
	Aging temperature /°C		21	21	21	40
T^1	δ_{iso}	[ppm±0.5]	−48.6	−49.3	−48.3	−51.6
	I	[% ± 1]	~1	~2	~1	~1
T^2	δ_{iso}	[ppm±0.5]	−58.4	−58.0	−58.7	−58.4
	I	[% ± 1]	19.0	19	12	9
T^3	δ_{iso}	[ppm±0.5]	−66.8	−66.6	−66.8	−66.9
	I	[% ± 1]	39	34	45	46
Q^2	δ_{iso}	[ppm±0.5]	−96.7	−95.9	-	−97.0
	I	[% ± 1]	1	1	-	~1
Q^3	δ_{iso}	[ppm±0.5]	−102.1	−1017	−102.5	−102.5
	I	[% ± 1]	8	9	11	8
Q^4	δ_{iso}	[ppm±0.5]	−111.3	−111.0	−111.5	−111.7
	I	[% ± 1]	32	35	32	36
D$_c$	[% ± 1]		**91**	**90**	**94**	**95**

3.2 3D printed scaffold architecture evolution

Two methods for drying the 3D printed hybrids were compared: freeze-drying (FD), which was the initial method used to sol-gel hybrid foams [20]; and critical point drying. FD avoids the transition from liquid to gas when removing aqueous solvent from a frozen material, as water is removed from the scaffold by sublimation of ice, which reduces the large shrinkage that would occur in ambient drying, but capillary stresses are experienced.

CPD is a drying technique which eliminates capillary stresses by avoiding the effects of liquid surface tension [37], but for the silica/gelation system, a solvent exchange was required, to pure ethanol. The ethanol is in turn replaced with liquid CO_2. When the temperature (31.1°C) and pressure (1170 psi) are elevated above the critical point, the CO_2 liquid and

vapour states are indistinguishable and in this super-critical state have the same density and surface tension. The liquid is then heated to convert the liquid to the gas phase without any distortion of the morphology. Gelatin alone is typically not compatible with this process, due to precipitation in ethanol, however in a hybrid system with covalent coupling, shrinkage rather than precipitation was predicted.

As a result, freeze drying (FD) and critical point drying (CPD) produced scaffolds with different overall size, strut width and channel size, even though the same printing fidelity of a 200 μm nozzle (nominal strut width) and 1 mm strut separation (nominal channel width) were used. SEM images (x,y plane) and μCT reconstructions presented in Figure 4 show that all scaffolds comprised of open channels and vertical walls in the vertical z (build) direction clearly seen in the FD scaffolds (Figure 4a, b, e, f). Horizontal channels were clear in the FD scaffolds (Figure 4c), similar to the z orientation, but were smaller and lower in number in the CPD scaffolds (Figure 4g). Negative 3D representations made by filling the pores and removing the scaffold, in the 3D image processing (Figure 4d and Figures 4h,i), showed high connectivity of pores in the FD scaffolds but more oriented pore channels in the z direction for the CPD scaffolds.
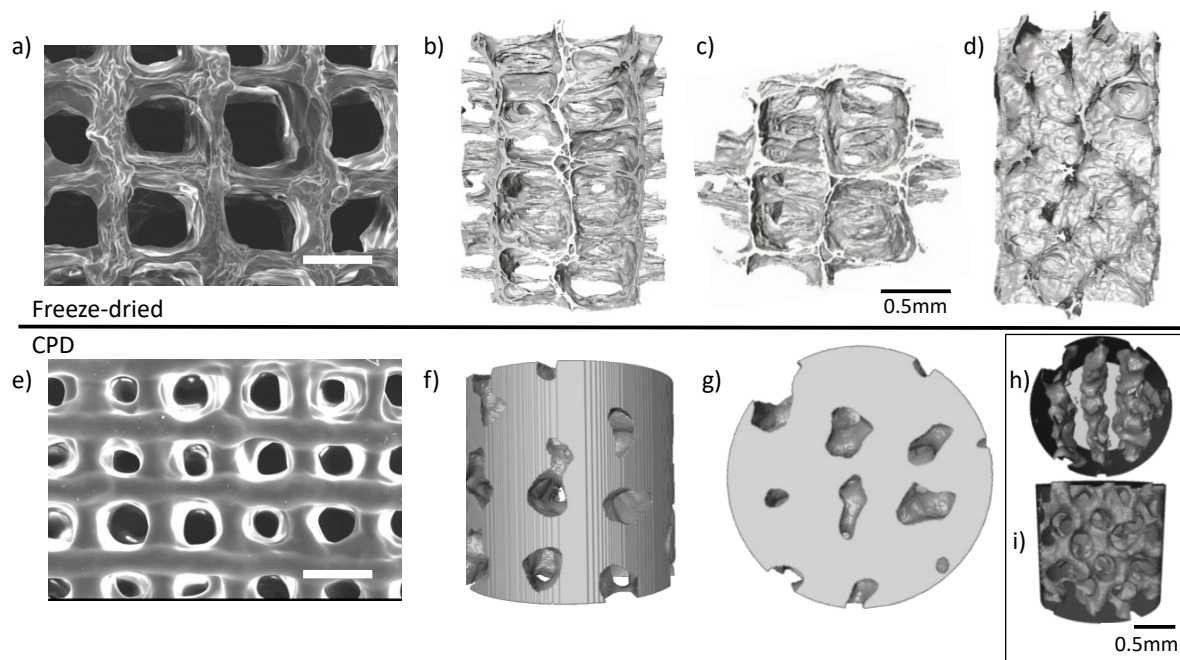

Figure 4. Imaging of 3D printed hybrid scaffolds using two drying methods: a-d) Freeze-dried, FD and e-i) critical point dried, CPD: (a,e) SEM images in the z direction of the x,y plane, scale bar is 500 μm; (b, c, d, f, g) μCT 3D reconstructions of scaffolds; (h,i) μCT 3D reconstructions of porosity (negative image). μCT images of scaffolds are viewed in the y,z (b,f), x,y (c,g,h) and x,z (d,i) plane (μCT images from Diamond Light Source).

In these 3D grid-like scaffolds, the term "channel size" is equivalent to the interconnected pore size in foam-like scaffolds. The channel size and strut sizes are summarised in Table 2. FD resulted in 682 ± 92 μm channels ("FD700") with < 40 μm struts whereas CPD resulted in 210 ± 53 μm channels ("CPD200") with 162 ± 27 μm struts. The porosity was calculated to be 88 % and 72 % for FD and CPD scaffolds respectively, using volume measurements and skeletal density values of 1.5 g cm^{-3} and 1.7 g cm^{-3} respectively in Equation 3. The porosity results seem to agree with Figure 4(h,i). The reduced pore channel size and increased strut thickness in the CPD was due to the increased shrinkage. Importantly, shrinkage was approximately isotropic, minimising distortion. The swelling of the scaffolds after 24 h in TRIS was therefore higher for CPD scaffolds than FD scaffolds, 156 ± 7 % versus 112 ± 3 % respectively.

Table 2. The mean channel width for FD and CPD scaffolds with 1 mm printed strut separation. Errors represent the standard deviation (30 struts and channels were measured over three samples).

Drying method	Shrinkage during drying/ %	Mean channel width/ μm	Mean strut width/ μm	φ, Porosity/ %	Scaffold ID
FD	42 ± 0	682 ± 92	<40	88 ± 1	FD700
CPD	80 ± 1	210 ± 53	162 ± 27	72 ± 0	CPD200

3.3 Dissolution study

In the dissolution study silicon release from the FD and CPD samples had a similar profile for the first 72 h (Figure 5) but total silicon release was less for CPD scaffolds (105 μm mL^{-1}) than for FD scaffolds (117 μm mL^{-1}). The gelatin release, ~ 32 μm mL^{-1}, was consistent independent of drying method.
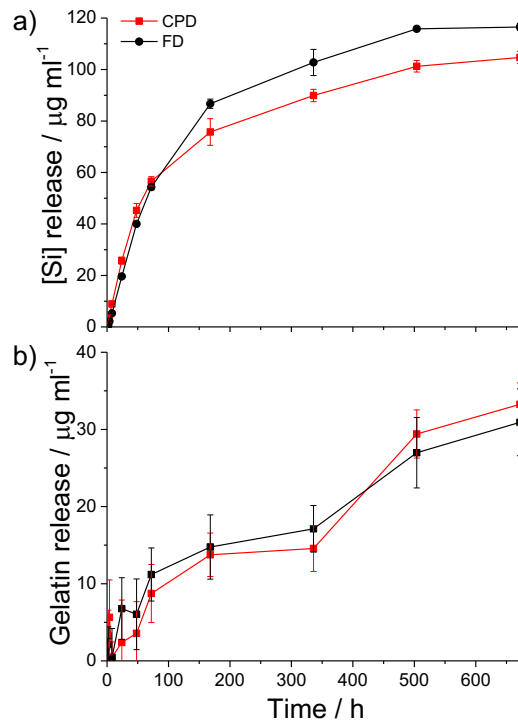
Figure 5. Dissolution profile in TRIS buffer for 3D printed hybrid scaffolds dried by freeze drying (FD700) and critical point drying (CPD200): concentration of a) silicon; b) gelatin.

The silicon and gelatin release was calculated as a percentage of the initial inorganic (hydrolysed TEOS and GPTMS silanol groups) and organic (gelatin and GPTMS organic chains) mass. The initial organic: inorganic ratio for CPD and FD scaffolds were 72:28 and 70:30 respectively as determined by TGA (Figure S3). For dissolution,150 mg of scaffold was used, hence for FD scaffolds, 45 mg was the inorganic and 105 mg was organic. Therefore 26 % of the total inorganic was released as silicon species and 3 % of the total organic content of the scaffold was released as gelatin. For CPD scaffolds dissolution was similar with 25 % of the inorganic released and 3 % of the organic released. After the one month study, the scaffolds had not changed in appearance as the low gelatin release resulted in volume stability of the scaffolds.

3.4 Compression testing

Representative plots of the stress strain curve for each type of scaffold tested are shown in Figure 6 and Table 3 gives the mean values obtained from compression testing and compares to hyaline cartilage. It is important how scaffolds behave when immersed in body fluid, so mechanical properties were assessed after 1 week immersion in TRIS buffer. The compressive strength and Young's modulus of the FD700 reduced by ~90 %, from 1 MPa to 0.1 MPa, as result of the week immersion in TRIS, and compressive strain doubled, from 0.1 to 0.2, which is likely to be due to the dissolution of silica and swelling, which increased the

water content and reduced the scaffold density. The compressive strength of the wet CPD200 scaffolds was over 10 times greater (1.3 MPa) than that of the wet FD700 scaffolds (0.1 MPa) due to the increased strut/wall width and reduced percentage porosity, even though dissolution was similar (Figure 5). The Young's modulus of the wet FD700 scaffolds was 0.7 ± 0.1 MPa, which is within the range of hyaline cartilage (0.5-1.0 MPa). As seen in Figure 6, the FD scaffolds had an approximately linear stress-strain relationship before yield, whereas CPD scaffolds showed a non-linear response.

Table 3. Mechanical properties hyaline cartilage and dry and wet (1 week immersion in TRIS) 3D printed scaffolds, made with 78G CF 500, dried via FD and CPD (n = >6).

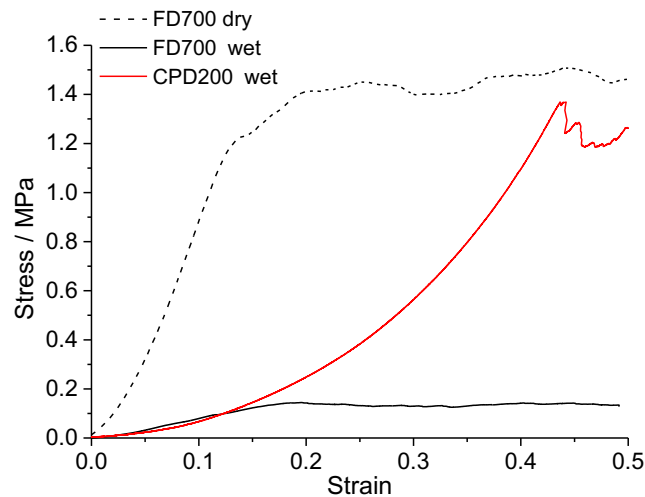| Sample	Compressive strength /MPa	Young's modulus, E /MPa	Compressive Strain
FD dry	1.0 ± 0.1	7.1 ± 0.9	0.1 ± 0.02
FD wet	0.1 ± 0.02	0.7 ± 0.1	0.2 ± 0.03
CPD wet	1.3 ± 0.04	n/a	0.5 ± 0.04
Hyaline cartilage	22-37 [38,39]	0.5 - 1.0 [40-42]	0.24-0.85 [40,43]

Figure 6. Example stress-strain plots of 3D printed hybrid scaffolds under compression: wet and dry FD700 scaffolds and wet CPD200 scaffolds. Solid lines indicate wet samples (1 week immersion in TRIS), dashed line indicates dry samples.

3.5 Cell studies

3.5.1 Biocompatibility and cell attachment

Results of MTT assays of ATDC5 chondrogenic cells and MCT3T3 pre-osteoblast cells, after exposure to the dissolution products of the 78G CF 500 scaffolds (Figure 7a), indicated the scaffolds can pass the ISO standards *in vitro* cytotoxicity of medical devices for biological device evaluation. An absorbance value less than 70% of that of the control/standard culture conditions would suggest cytotoxicity. Toxicity was only observed for the PU controls. The well organised actin and well-defined vimentin markers in Figure 7b indicate robust attachment of ATDC5 cells, which spread across the surface. MCT3T3 cells also attached to the scaffolds, as shown in Figure 7c.
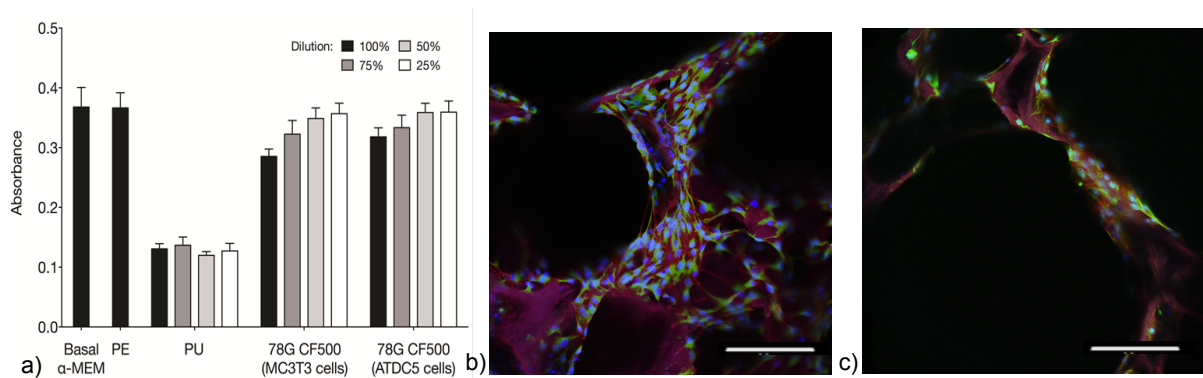
Figure 7. a) MTT metabolic activity assay according to the ISO standards 10993-5 and 10993-12. Dilution % values are vol% concentrations in basal media for ATDC5 chondrogenic cells and MCT3T3 osteoblast cells after 24 h culture (n=3). Confocal images of cells on the 3D printed scaffolds stained for cytoskeletal protein actin (red), vimentin (green) and nuclei (blue): (b) ATDC5 and (c) MCT3T3. Scale bars are 200 μm.

Cartilage matrix formation

The difference in channel size, brought about by the post printing drying method, affected ATDC5 cell behaviour (Figure 8). Cells cultured on the CPD200 demonstrated robust chondrogenic differentiation and hyaline-like cartilaginous matrix formation (Figure 8). Sox9, a marker for chondrogenic differentiation, was localised in the majority of cells. The dense extracellular matrix, which could occupy the entire pore structure, was composed of collagen Type II, a key marker for hyaline articular cartilage and cartilage specific aggrecan, the major non-collagenous component. Collagen Type II and aggrecan were sparse in the FD700 scaffold with larger pores. However, the expression of collagen Type I, a marker for fibrocartilage (among other tissues), was present in FD700 and not present in CPD200. Similar outcomes were shown for ATDC5 culture in other 3D printed hybrid scaffolds, in that case comparing ~200 μm channels with 500 μm channels of

silica/poly(tetrahydrofuran)/polyTHF/poly(ε-caprolactone) hybrids [28]. Here, to determine whether increasing the seeding cell number, for the freeze-dried scaffolds with 700 μm pore channels, would improve cell-cell interactions, the number of cells seeded was increased to 10×10^6. Collagen Type II and aggrecan were highly expressed at the increased cell density, but the presence of collagen Type I in FD700 scaffolds persisted.
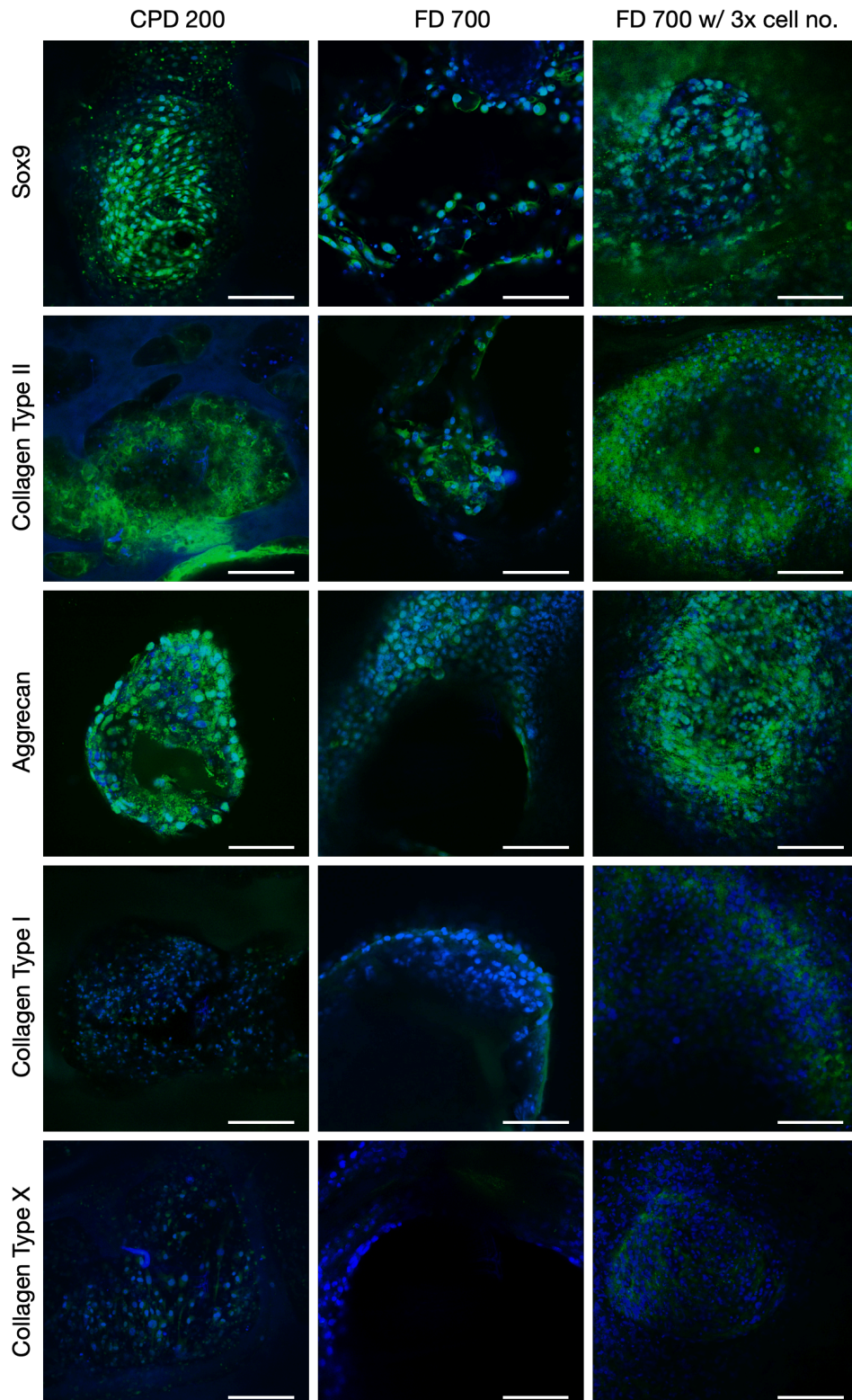
Figure 8. Confocal images of ATDC5 cells cultured in the 3D printed scaffolds that were: critical point dried with a 200 μm pore channel size (CPD200); freeze dried (FD) with a 700 μm pore channel size (FD700) and the FD700 scaffolds with a 3x higher seeding cell number. Staining was for cytoskeletal proteins at 28 days of culture: Sox9, collagen type II, aggrecan, collagen type I, collagen type X (all green) and nuclei (blue). Scale bars are 200 μm.

The gene expression analysed by quantitative PCR in Figure 9 confirmed the observations from immunohistochemical staining. *Sox9, COL2a1 and Aggrecan* were all expressed significantly more by ATDC5 cells cultured in the scaffolds with 200 μm channels than in scaffolds with 700 μm channels, when the same number cells were used. When the cell number was tripled in the FD700 scaffolds, the expression of *Sox9* on CPD200 and FD700 (with high seeding cell numbers) scaffolds were similar, but the levels of cartilage matrix specific gene *Col2a1* and *Aggrecan* were still significantly higher for cells cultured on CPD200 scaffolds. The expression of *Col1a1* by ATDC5 cells on FD700 scaffolds was significantly higher in comparison to those on CPD200 scaffolds, even with the similar cell density. The level of *Col10a1* was similar in all three conditions, however, it should be noted that the C_T values were in the range of 29 to 31, indicating the expression of *Col10a1* gene can be regarded as negligible.
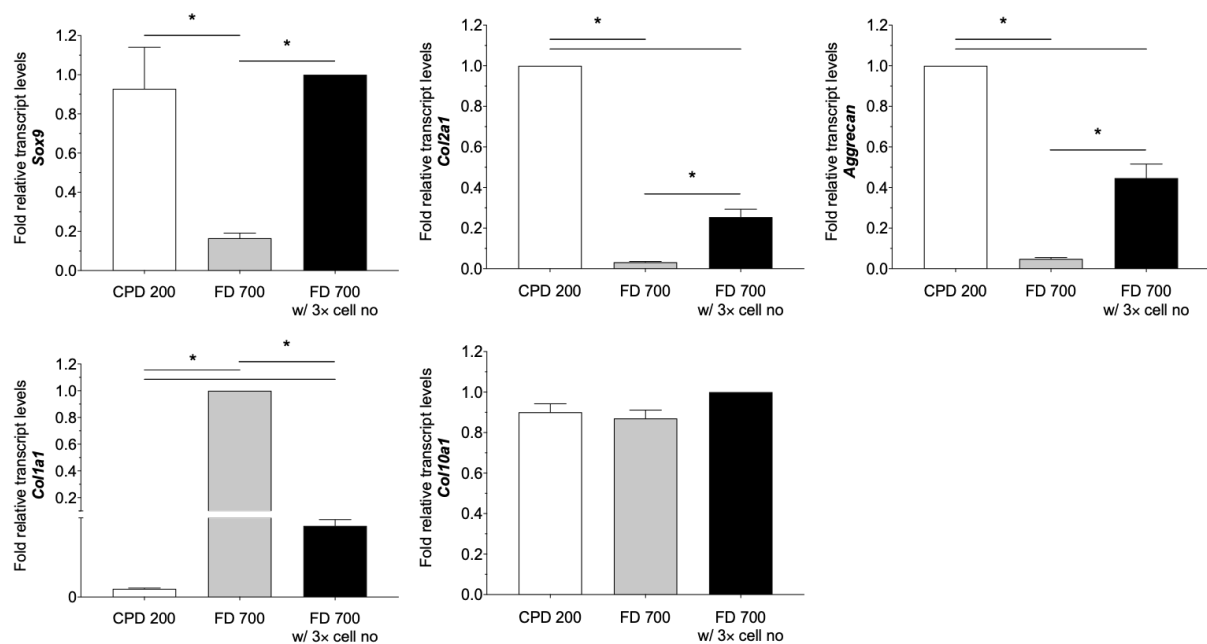

Figure 9. qPCR analysis of gene expression (*Sox9*, *Col2a1*, *Aggrecan*, *Col1aI*, *Col10a1*) from ATDC5 cells cultured for 28 days on the 3D printed scaffolds including: critical point dried (CPD) with a 200 μm pore channel size (CPD200); freeze dried (FD) with a 700 μm pore channel size (FD700) and the FD700 scaffolds seeded with a 3× higher cell number. The results were normalised to the transcript level of GAPDH housekeeping gene. Fold relative transcript

level of target gene was calculated using comparative ΔC_T method (i.e. $2^{-\Delta\Delta C_T}$) and the group with the highest relative transcript level was assigned to a value of 1. Statistical analysis was performed at the level of ΔC_T. n= 3 and * indicates p < 0.05.

The formation of glycosaminoglycan, the main non-collagenous component of cartilage matrix, was also appears more efficient on CPD200 scaffolds compared to FD700 as shown in Figure 10. Only by increasing the cell seeding number did the GAG levels of the cells within the FD700 scaffold reach those cultured in the 200 µm pore channels.
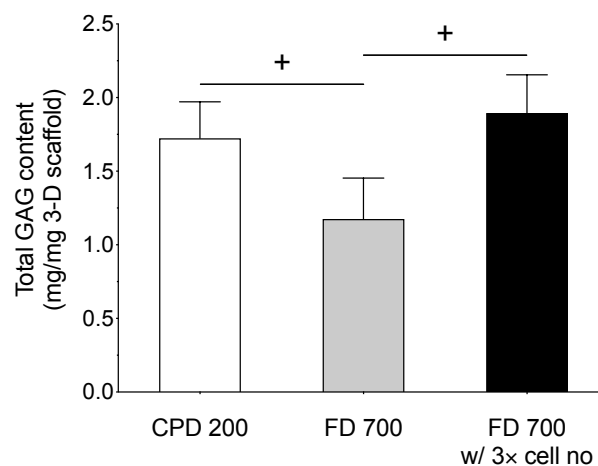
Figure 10. Quantitative glycosaminoglycan (sGAG) assay after 28 days of ATDC5 cells culture in scaffolds FD700, CF200 and FD700 with 3x the cell number. n=3 and + indicates 0.05 < p < 0.1.

Discussion

The hybrid ink composition chosen was 78G CF 500. A CF of 500 was selected as increasing the CF above this value did not further improve the crosslinking in the hybrid. This was not due to saturation of functionalisation sites on the gelatin molecules as CF 500 corresponds to a molar ratio of GPTMS to amino acids involved in functionalisation (glutamic and aspartic acid) of 0.27 [44,45]. It is likely the kinetics of the reaction slowed, due to reduced availability of binding sites and oligomer formation above this ratio of GPTMS to gelatin. The ink composition found most suitable for 3D printing via this Direct Ink Writing extrusion method was 78G CF 500, due to the convenient gelation rate and large printing window. The rate of silica network condensation was reduced as gelatin content increased and increasing the GPTMS could not compensate for the reduction in TEOS content and gel strength.

A combination of the ninhydrin assay and solid state NMR results showed that covalent coupling between the gelatin and silica network was successful, using GTPMS, and reducing

the functionalisation time for gelatin with GPTMS form 14 h to 3 h had little effect on D_c and the D_c was similar to that of the sol-gel foaming method [20].

The structure and properties of 3D printed scaffolds dried via CPD were found to be preferable for cartilage tissue regeneration. CPD scaffolds produced channels with widths of 210 µm, which was similar to channel sizes for other hybrid scaffolds shown to support hyaline articular-cartilage-like matrix formation *in vitro* [28,29], which agrees with earlier hypotheses on the ideal 3D environment for cartilage cells [46]. The FD scaffolds had pore channels that were over three times larger: 682 µm. Using CPD, the scaffolds retained rounded struts with a mean width of 162 µm, whereas during FD struts shrank to < 40 µm and appeared to be fragmented (Figure 4), perhaps due to ice crystals forming in the struts during freezing, which were then removed in the freeze drying, without allowing consolidation of the struts by continued gelation. In fact, the struts were similar to the thin pore walls that resulted from the sol-gel foaming process, which also employed freeze-drying [20].

The low degree of swelling (156 % for CPD and 114% for FD scaffolds) showed considerable improvement on the hybrids 3D printed by Gao *et al.* (440 % swelling in just 2 h). The low swelling was due to the high degree of covalent coupling, which prevented water from entering the gelatin network [47]. The success of the covalent coupling was confirmed by solid state NMR and the ninhydrin assay. However, the coupling may have been less than achieved previously in the sol-gel foaming process [20]. Here, despite a similar degree of silica network condensation (D_c), T^1 and T^2 increased at the expense of T^3 in the 3D printed scaffolds, compared to the foams. This reduced coupling may benefit low stiffness applications, such as cartilage regeneration.

Under compressive loading, the scaffolds dried using CPD had a compressive strength (1.3 ± 0.04 MPa) approximately ten times that of FD scaffolds (0.1 ± 0.02 MPa), due to the increased strut/wall width and reduced total porosity. The strain-strain response of the CPD scaffolds was non-linear displaying increased stiffness with increased loading, a viscoelastic response similar to native hyaline cartilage [43] [48], whereas the FD scaffold exhibited a linear stress-strain response. The change in behaviour is predicted to arise from the higher degree of swelling of the CPD scaffolds and larger strut width which allowed densification of the material during compression by expulsion of water molecules from the gelatin network. As shown in Figure 7, organisation of actin and vimentin are well defined in ATDC5 cells in comparison to MC3T3 cells. This could be due to the scaffold having a lower stiffness than bone matrix [41], again confirming the 78G CF 500 is a more suitable substrate for cartilage regeneration applications.

The pore channel size affected the type of matrix produced in the scaffolds during cell culture *in vitro*. After 28 days of culture in the CPD200 scaffolds, ATDC5 chondrocytes demonstrated robust chondrogenic differentiation and hyaline-like cartilaginous matrix formation in CPD200 scaffolds compared to those cultured in FD700 scaffolds. Immunohistochemistry (Figure 8) and gene expression analyses (Figure 9) confirmed significantly increased expression of both protein and gene expression of relevant markers in CPD200 scaffolds, including Sox9, Collagen Type II and Aggrecan. There was noticeable expression of Collagen Type I in FD700 scaffolds, an indication of undesirable fibrous tissue formation, this was not present in CPD200 scaffolds. Formation of sulphated GAG was also parse in FD700 scaffolds. Collagen Type X was negligible in all culture conditions. These results indicate that hyaline-like cartilage matrix was produced when cells were cultured in a structure with 200 μm pore channels, but when the pore channel size increased, the cells produced fibrocartilage-like matrix. This could be due to the type of cell-cell interactions within the pore channels.

The pore architecture, such as porosity, pore size and interconnectivity, of a scaffold are influential in controlling cell distribution, mass transportation via diffusion and chondrogenic differentiation [49]. The 3D printed 78G CF 500 scaffolds contained approximately 72 % (CPD) and 88 % (FD) porosity, which may have contributed to the sufficient mass exchange during the prolonged culture period. Similar results were seen previously in silica/poly(tetrahydrofuran)/polyTHF/poly(ε-caprolactone) hybrids [28,29]. The hypothesis was that pore channels that have widths of ~200-250 μm allow chondrocytes to have 3D cell-cell interactions, whereas in the larger pores (e.g. > 500 μm) the cells flatten against the scaffold struts/ pore walls and dedifferentiate into fibroblasts [29]. Here, in the larger pores, the cells may be in too low a density for 3D interactions. They may flatten to the surface of the struts, as was seen for MSCs on other hybrid scaffolds [29]. This was tested by increasing the cell number. While the difference between the scaffold types was less, there the fibrocartilage matrix markers (collagen Type I) still dominated.

The exact effects of pore size on the formation of cartilaginous matrix remain inconclusive and further studies are needed to investigate this hypothesis, however, previous work has shown in scaffolds containing smaller pores, chondrocytes reach higher cell density and cell-cell interactions were improved, resulting in enhanced cell proliferation, GAG and collagen content [50,51]. Pore size could affect cell spreading due to the amount of available surface area for cells. It has been demonstrated for fibroblasts that the extent of cell spreading plays an important role in activation of signal transduction mechanism and the subsequent cellular behaviour [52] and when chondrocytes attach and spread in a 2D environment, they can

undergo dedifferentiation, resulting in Collagen Type I production [53-55]. Indeed, notably increased amount of Collagen Type I was observed in cells cultured in FD 700 scaffolds with larger pores (700 µm). It is likely that, cells cultured in the larger pores experienced environments closer to 2D culture, spreading along the struts/ pore walls, resulting in increased chondrocyte dedifferentiation.

Higher cell density may also have caused decreased apoptosis, another mechanism that likely contributed to increased cartilaginous tissue formation. It has been shown that aggregated chondrocytes (similar to those resides in small pores) demonstrated a significant decrease in the number of cells undergoing apoptosis [56]. Increasing the seeding cell number in the FD700 scaffolds appeared to improve chondrogenic differentiation to a level comparable to CPD200 scaffolds, as evidenced by *Sox9* gene expression. The formation of cartilaginous matrix however remain suboptimal with the persistent existence of Collagen Type I. It should also be noted that in clinical settings, it is not always feasible to achieve high cell number especially in patients whose cartilage is already severely damaged and/or those with other underlying diseases.

Conclusion

Silica-gelatin sol-gel Class II hybrids were developed as new biomaterial inks for 3D printing for use in combination with microfracture surgery to encourage functional hyaline articular cartilage regeneration. The 78G CF 500 hybrids were compatible with an optimised 3D printing protocol, which avoided rapid gelation, but retain high levels of coupling and sol-gel network condensation. Critical point drying and freeze drying were compared as drying techniques after printing. The 3D printed scaffolds showed a low degree of swelling in buffer solutions. Critical point drying produced scaffolds with mechanical properties close to native cartilage and pore channels of ~200 µm proved capable of supporting hyaline-like cartilaginous matrix formation, in terms of collagen type II, Sox9 and Aggrecan production *in vitro,* with little collagen type I or X expression.

ACKNOWLEDGEMENTS
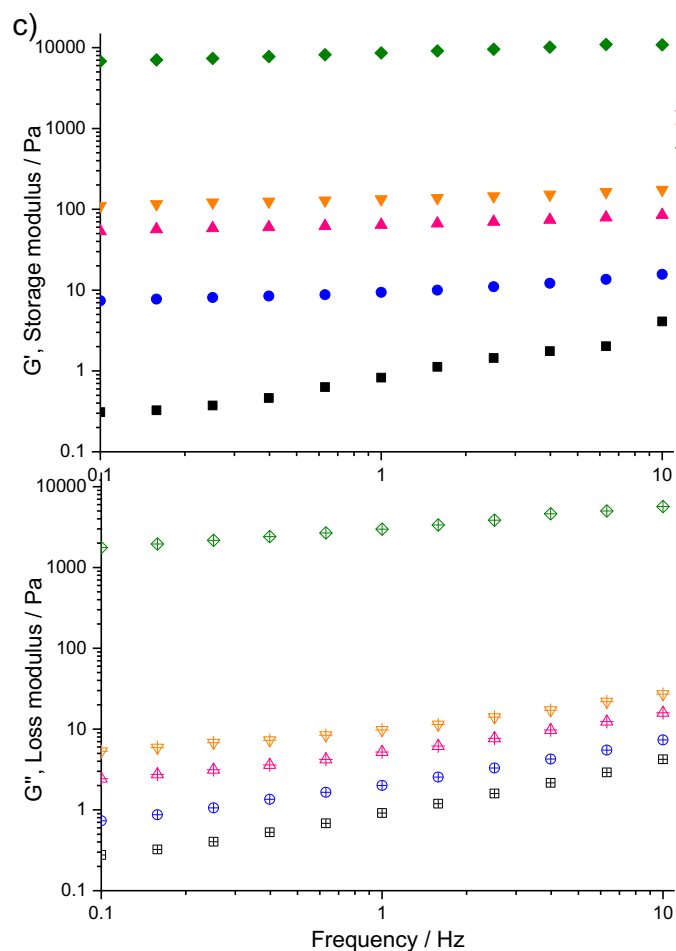
Supplementary information

Figure S1. Storage and loss moduli of 78G CF 500 hybrid gels measured using oscillation-frequency tests between 7 h and 15 h after mixing the hybrid components. The rheology of the 78G CF 500 hybrids was monitored during the solution aging period, within the 3D printing window, and after the solution had become too gelled for printing. The plots of the storage and loss modulus indicate a highly crosslinked gel with no shear thinning behaviour.
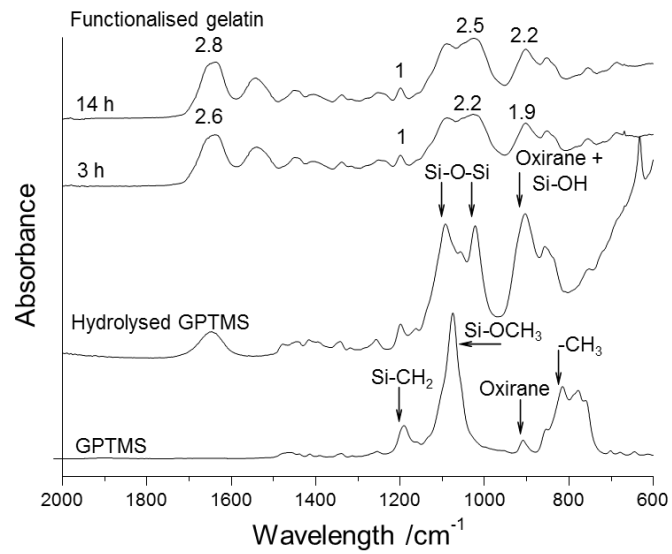
Figure S2. FTIR spectra of GPTMS before and after hydrolysis and gelatin functionalised by GPTMS for 3 h and 14 h. Band ratios are displayed relative to the Si-C band.
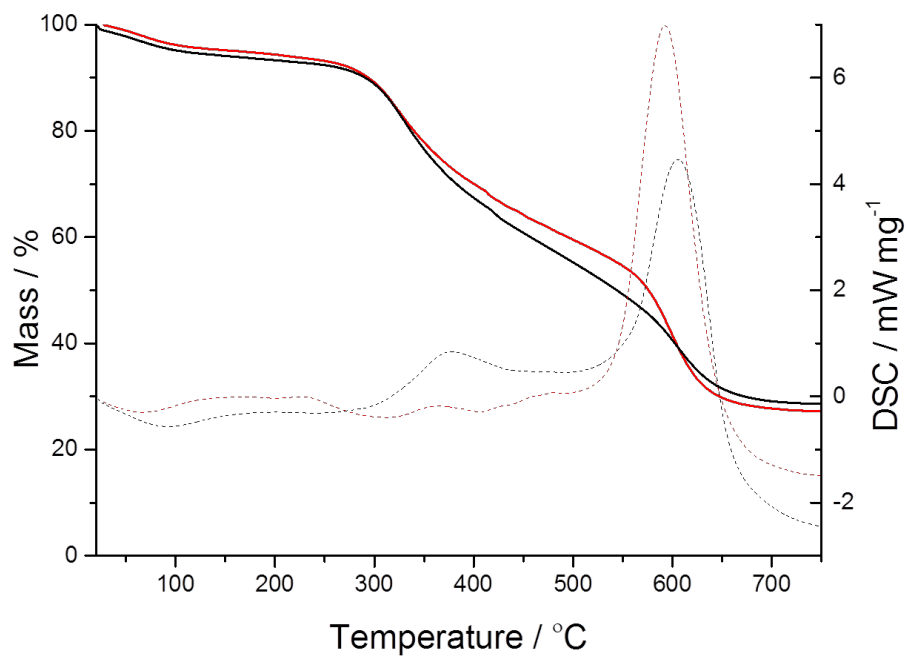

Figure S3. TGA and DSC analysis comparing hybrid 78G CF500 scaffolds dried via FD and CPD.

References

1.   Mithoefer, K*., et al.*, *Am. J. Sports Med.* (2009) **37** (10), 2053
2.   Goldring, M. B., *Therapeutic Advances in Musculoskeletal Disease* (2012) **4** (4), 269
3.   Oliveria, S. A*., et al.*, *Arthritis and Rheumatism* (1995) **38** (8), 1134
4.   Steadman, Jr., and Sterett, W. I., *Med. Sci. Sports Exerc.* (1995) **27** (3), 328
5.   Giannini, S*., et al.*, *Injury* (2010) **41** (11), 1196
6.   Benthien, J. P., and Behrens, P., *Knee Surg Sports Traumatol Arthrosc* (2011) **19** (8), 1316
7.   Gille, J*., et al.*, *Knee Surg Sports Traumatol Arthrosc* (2010) **18** (11), 1456
8.   Schagemann, J*., et al.*, *Arch Orthop Trauma Surg* (2018) **138** (6), 819
9.   Baba, R*., et al.*, *Am J Sports Med* (2018) **46** (8), 1970
10.   Almeida, H. V*., et al.*, *Tissue Eng Part A* (2017) **23** (1-2), 55
11.   Koh, Y. G*., et al.*, *J. Tissue Eng.* (2019) **10**
12.   Kwan, H*., et al.*, *Materials* (2020) **13** (2)
13.   Setayeshmehr, M*., et al.*, *Tissue Eng. Part B* (2019) **25** (3), 202
14.   Camarero-Espinosa, S*., et al.*, *Biomater. Sci.* (2016) **4** (5), 734
15.   Vunjak-Novakovic, G*., et al.*, *Biotechnology Progress* (1998) **14** (2), 193
16.   Sobral, J. M*., et al.*, *Acta Biomater* (2011) **7** (3), 1009
17.   Dong, C. J., and Lv, Y. G., *Polymers* (2016) **8** (2)
18.   Ito, A*., et al.*, *Journal of Bioscience and Bioengineering* (2003) **95** (2), 196
19.   Kirchmajer, D. M., and Panhuis, M. I. H., *J. Mat. Chem. B* (2014) **2** (29), 4694
20.   Mahony, O*., et al.*, *Adv. Funct. Mater.* (2010) **20** (22), 3835
21.   Mahony, O*., et al.*, *J. Sol-Gel Sci. Technol.* (2014) **69** (2), 288
22.   Jones, J. R., *Acta Biomater* (2013) **9** (1), 4457
23.   Poologasundarampillai, G*., et al.*, *Soft Matter* (2012) **8** (17), 4822
24.   Keri, M*., et al.*, *Acta Biomater* (2020) **105**, 131
25.   Veres, P*., et al.*, *J. Non-Cryst. Solids* (2017) **473**, 17
26.   Greenhalgh, R. D*., et al.*, *J. Mater. Sci.* (2017) **52** (15), 9066
27.   Gao, C*., et al.*, *J. Biomed. Mater. Res. Part A* (2013) **101** (7), 2027
28.   Tallia, F*., et al.*, *Mater Horiz* (2018) **5**, 849
29.   Li, S*., et al.*, *Biomater. Sci.* (2020)
30.   Lai, J. Y*., et al.*, *PLoS One* (2013) **8** (1)
31.   Poologasundarampillai, G*., et al.*, *J. Mater. Chem.* (2010) **20** (40), 8952
32.   Maçon, A. L. B*., et al.*, *Journal of Materials Science: Materials in Medicine* (2015) **26** (2), 115
33.   Mackay, A. M*., et al.*, *Tissue Eng.* (1998) **4** (4), 415
34.   Li, S*., et al.*, *J Biomater Appl* (2015) **29** (6), 824
35.   Knight, M. M*., et al.*, *Biochimica Et Biophysica Acta-Molecular Cell Research* (1998) **1405** (1-3), 67
36.   Fu, Q*., et al.*, *Acta Biomater* (2011) **7** (10), 3547
37.   Weibel, G. L., and Ober, C. K., *Microelectronic Engineering* (2003) **65** (1-2), 145
38.   Kerin, A. J*., et al.*, *Proceedings of the Institution of Mechanical Engineers Part H-Journal of Engineering in Medicine* (1998) **212** (H4), 273
39.   Repo, R. U., and Finlay, J. B., *Journal of Bone and Joint Surgery-American Volume* (1977) **59** (8), 1068
40.   Jurvelin, J. S*., et al.*, *Journal of Biomechanics* (1997) **30** (3), 235
41.   Allen, J. L*., et al.*, *Molecular Biology of the Cell* (2012) **23** (18), 3731
42.   Li, S. W*., et al.*, *Lab Chip* (2014) **14** (23), 4475
43.   Little, C. J*., et al.*, *Tissue Eng. Part B* (2011) **17** (4), 213
44.   Farris, S*., et al.*, *Journal of Agricultural and Food Chemistry* (2010) **58** (2), 998
45.   Connell, L. S*., et al.*, *Polym. Chem.* (2017) **8** (6), 1095
46.   Woodfield, T. B*., et al.*, *Tissue Eng* (2005) **11** (9-10), 1297

47. Ren, L.*, et al.*, *Biomaterials* (2002) **23** (24), 4765
48. Edelsten, L.*, et al.*, *Soft Matter* (2010) **6** (20), 5206
49. Nuernberger, S.*, et al.*, *Biomaterials* (2011) **32** (4), 1032
50. Bhardwaj, T.*, et al.*, *J Biomed Mater Res* (2001) **57** (2), 190
51. Oh, S. H.*, et al.*, *Biomaterials* (2007) **28** (9), 1664
52. Defilippi, P.*, et al.*, *Microscopy Research and Technique* (1999) **47** (1), 67
53. Vondermark, K.*, et al.*, *Nature* (1977) **267** (5611), 531
54. Kino-Oka, M.*, et al.*, *Tissue Eng.* (2005) **11** (3-4), 597
55. Caron, M. M. J.*, et al.*, *Osteoarthritis and Cartilage* (2012) **20** (10), 1170
56. Cao, L., and Yang, B. B., *Experimental cell research* (1999) **246** (2), 527